University of Groningen

Vacuolar Localization via the N-terminal Domain of Sch9 is Required for TORC1-dependent Phosphorylation and Downstream Signal Transduction

Novarina, Daniele; Guerra, Paolo; Milias-Argeitis, Andreas

[Link to publication in University of Groningen/UMCG research database](#)

Vacuolar Localization via the N-terminal Domain of Sch9 is Required for TORC1-dependent Phosphorylation and Downstream Signal Transduction

Daniele Novarina, Paolo Guerra and Andreas Milias-Argeitis *

Molecular Systems Biology, *Groningen Biomolecular Sciences and Biotechnology Institute, University of Groningen, Nijenborgh 4, 9747 AG Groningen, the Netherlands*

Correspondence to Andreas Milias-Argeitis: a.milias.argeitis@rug.nl *(A. Milias-Argeitis)*
@andreas_milias 🐦 *(A. Milias-Argeitis)*
https://doi.org/10.1016/j.jmb.2021.167326
Edited by Lutz Schmitt

Abstract

The budding yeast Sch9 kinase (functional orthologue of the mammalian S6 kinase) is a major effector of the Target of Rapamycin Complex 1 (TORC1) complex in the regulation of cell growth in response to nutrient availability and stress. Sch9 is partially localized at the vacuolar surface, where it is phosphorylated by TORC1. The recruitment of Sch9 on the vacuole is mediated by direct interaction between phospholipids of the vacuolar membrane and the region of Sch9 encompassing amino acid residues 1-390, which contains a C2 domain. Since many C2 domains mediate phospholipid binding, it had been suggested that the C2 domain of Sch9 mediates its vacuolar recruitment. However, the *in vivo* requirement of the C2 domain for Sch9 localization had not been demonstrated, and the phenotypic consequences of Sch9 delocalization remained unknown. Here, by examining cellular localization, phosphorylation state and growth phenotypes of Sch9 truncation mutants, we show that deletion of the N-terminal domain of Sch9 (aa 1-182), but not the C2 domain (aa 183-399), impairs vacuolar localization and TORC1-dependent phosphorylation of Sch9, while causing growth defects similar to those observed in Sch9Δ cells. These defects can be reversed either via artificial tethering of the protein to the vacuole, or by introducing phosphomimetic mutations at the TORC1 target sites, suggesting that Sch9 localization on the vacuole is needed for the TORC1-dependent activation of the kinase. Our study uncovers a key role for the N-terminal domain of Sch9 and provides new mechanistic insight into the regulation of a major TORC1 signaling branch.

Introduction

The Sch9 kinase is a functional orthologue of the mammalian S6 kinase[1] which regulates many different aspects of budding yeast growth, such as ribosome biogenesis, translation initiation, entry into G0, sphingolipid metabolism, stress resistance and longevity.[1–7] Sch9 is also a well-characterized substrate and major effector of the highly conserved Target of Rapamycin Complex 1 (TORC1), an essential multiprotein complex which controls cell growth in response to various nutrient and stress cues,[8] and TORC1-dependent phosphorylation of Sch9 at several C-terminal residues is required for Sch9 activity.[1] The central role that Sch9 plays in cell growth is evidenced by the fact that Sch9Δ cells are small and divide slowly on glucose,[9,10] while they fail to grow altogether on non-fermentable carbon sources.[1,11]

Sch9 is found in the cytoplasm, but is also enriched on the vacuolar membrane,[1,12–14] where yeast TORC1 predominantly resides.[15–17] Previous work[18] had shown that Sch9 is recruited to the vacuole in a PI(3,5)P2-dependent manner via a region containing amino acid residues 1-390. Since this region contains the C2 domain of Sch9 (Figure 1
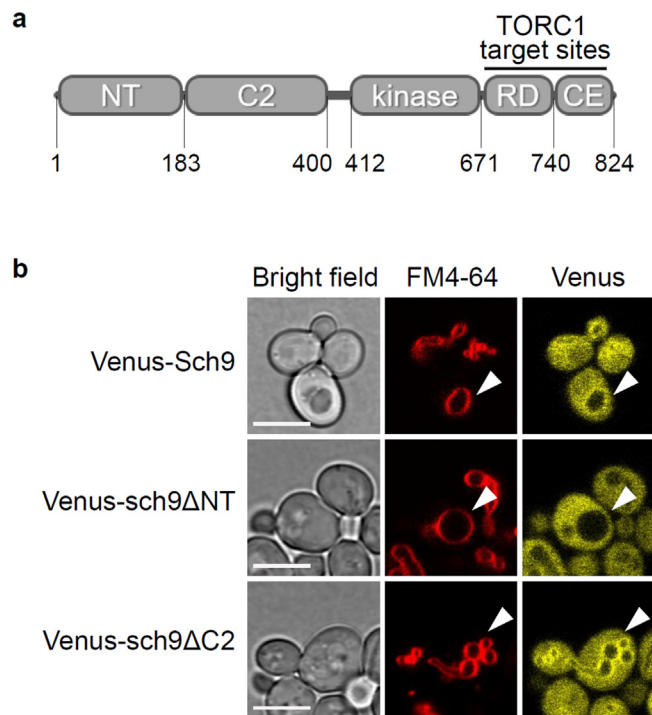
Figure 1. Recruitment of Sch9 at the vacuolar membrane is mediated by its N-terminal domain. (a) Schematic representation of Sch9 domains. NT, N-terminal domain; C2, C2 domain; kinase, kinase domain; RD, regulatory domain; CE, C-terminal extension. (b) Localization of Venus-tagged Sch9 truncation mutants in unperturbed cells. Vacuole membranes were stained with FM4-64. Sch9 is partially localized on the vacuole in wild-type and Sch9ΔC2, but not in Sch9ΔNT. Scale bar, 5 μm. Further microscopy images, as well as quantification of Venus fluorescence can be found in Figure S1.

(a)) and C2 domains often bind phosphoinositide lipids,[19] it was thought that the C2 domain mediates binding of Sch9 to the vacuole. However, the *in vivo* requirement of the C2 domain for vacuolar localization of Sch9 has not been demonstrated. More importantly, while the vacuolar fraction of the protein disappears under carbon starvation[12] and oxidative stress[20] when cell growth is inhibited, it remains unclear if the capability of Sch9 to bind to the vacuole is a prerequisite for downstream signal transduction under favorable growth conditions, as the growth phenotype induced by specific disruption of Sch9 localization has not been documented.

In this work, we demonstrate that the Sch9 fragment containing the C2 domain (residues 183-399) is fully dispensable for the vacuolar localization of the protein, which instead relies on its N-terminal domain (residues 1-182) to attach to the vacuole. Deletion of this N-terminal domain (but not deletion of the C2 domain) greatly decreased the phosphorylation of Sch9 by TORC1 under rich nutrient conditions, and resulted in a growth phenotype very similar to that of Sch9Δ. Remarkably, growth defects induced by N-terminal truncation of Sch9 could be reversed by artificially tethering this mutant to the vacuole, or by introducing phosphomimetic mutations at the TORC1-dependent residues. Collectively, our results demonstrate that vacuolar localization of

Sch9 is a major component of the activation mechanism and downstream activity of the kinase, and provide new insights on the functionality of this central regulator of cell growth.

Results

The N-terminal domain of Sch9 is necessary for its localization on the vacuole

Previous work had suggested that Sch9 localizes on the vacuole via the interaction of its C2 domain with the signaling phospholipid phosphatidylinositol 3,5-bisphosphate (PI(3,5) P2).[18] However, an Sch9 fragment (residues 1-390) which is much longer than the C2 domain (residues 183-399) was used to demonstrate binding to the vacuole *in vivo*.

To assess which fraction of the first 390 amino acids of Sch9 is responsible for its recruitment at the vacuole, we stained the vacuolar membrane with FM4-64[21] and compared via fluorescence microscopy the *in vivo* localization of different Venus-tagged Sch9 truncations with the localization of full-length Sch9. As reported in the literature, Sch9 was found both in the cytoplasm and the vacuolar membrane (Figures 1(b) and S1). We observed that, while deletion of the N-terminal domain (residues 1-182) abrogated the vacuolar

localization of Sch9, the Sch9ΔC2 protein (missing residues 183-399) was still able to localize on the vacuolar membrane (Figures 1(b) and S1). Altogether, these observations imply that the C2 domain is dispensable for Sch9 recruitment at the vacuole, contrary to what had been suggested by Jin et al.[18] Instead, the vacuolar recruitment of Sch9 is mediated by its N-terminal domain.

Vacuolar localization of Sch9 via the N-terminal domain is necessary for its TORC1-dependent phosphorylation

Given that a large fraction of yeast TORC1 resides on the vacuole, we next investigated the phosphorylation of the truncated Sch9 mutants. Previous work[1,20] had shown that an Sch9 C-terminal fragment containing all TORC1-dependent phosphorylation sites (Sch9[709-824]) was indeed phosphorylated by TORC1 when tethered on the vacuolar membrane, whereas a cytosolic version of the same fragment was not phosphorylated. To investigate whether similar conclusions hold for our Sch9 truncation mutants, we created C-terminally HA-tagged versions of these mutants and examined their TORC1-dependent phosphorylation in comparison to wild-type Sch9 by SDS-PAGE and Western blot. To facilitate the analysis of the wild-type and truncated versions of Sch9 which have different sizes, we treated protein extracts with NTCB (2-nitro-5-thiocyanatobenzoic acid), which cleaves Sch9 at specific cysteine residues. This treatment allows the analysis of a C-terminal fragment of Sch9 that contains all TORC1 phosphorylation sites[1] and has the same length in all of our mutants (Figure 2(a)). We observed that,

while wild-type Sch9 is phosphorylated in exponentially growing cells, deletion of the Sch9 N-terminal domain resulted in almost complete loss of TORC1-dependent phosphorylation, to a level comparable to that observed for wild-type Sch9 after TORC1 inhibition with rapamycin (Figure 2(b)). Conversely, phosphorylation of Sch9ΔC2 was unaffected (Figure 2(b)). The above analysis suggests that recruitment of Sch9 at the vacuolar surface via its N-terminal domain is necessary for its phosphorylation by TORC1. On the contrary, loss of the C2 domain does not affect Sch9 phosphorylation.

Cells lacking the N-terminal, but not the C2 domain of Sch9, exhibit growth defects

It is known that TORC1-dependent phosphorylation of wild-type Sch9 is necessary for its downstream activity, since an Sch9 mutant that cannot be phosphorylated by TORC1 displays phenotypic traits similar to Sch9Δ.[1] To investigate if the phosphorylation status of Sch9 truncation mutants also affects downstream signal transduction, we created strains carrying the truncation of the N-terminal or the C2 domain at the endogenous Sch9 locus and examined several cell growth-related features that are affected by deletion of the Sch9 gene. Given the central role that Sch9 plays in the coordination of growth and division[9,12] in both mother and daughter cells, we used single-cell time-lapse microscopy to quantify the following features for cells grown on YPD medium (cf. Methods): i) the time between divisions of a mother cell (defined as the interval between one budding event and the next) ii) the duration of the G1 phase in daughter
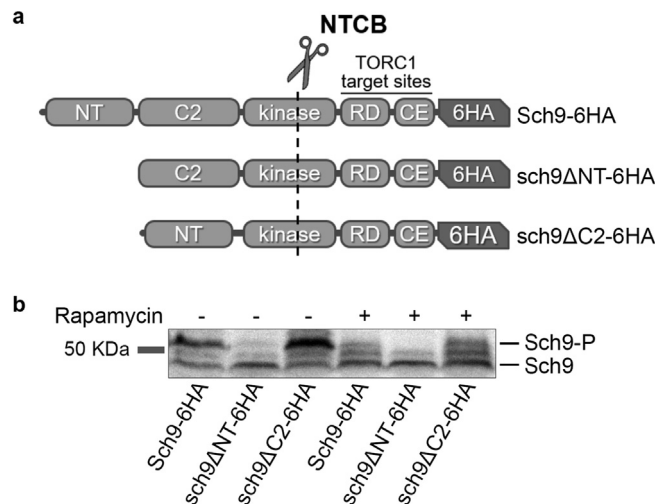
Figure 2. Deletion of the N-terminal domain impairs TORC1-dependent Sch9 phosphorylation. (a) Schematic representation of HA-tagged Sch9 truncation mutants. The dashed line indicates the most HA-proximal NTCB cleavage site. (b) Protein extracts from mock- or rapamycin- treated yeast cultures expressing HA-tagged wild-type Sch9 or the indicated truncation mutants were subjected to chemical fragmentation with NTCB and analyzed by Western Blotting using anti-HA antibodies.[1]

cells (defined as the interval between detachment of the bud from the mother cell and the following budding event) iii) the volume of daughter cells at birth and at the first budding event (Figure 3(a)). These features were used to assess the functionality of the mutant Sch9 forms compared to wild-type Sch9 and Sch9Δ. In our tests, Sch9ΔNT displayed a growth phenotype that was very similar to Sch9Δ[10]: the time between mother cell divisions and the G1 duration of daughter cells increased to the Sch9Δ levels (Figure 3(b), (c) and Table 1), while the size of daughter cells at birth and at budding decreased to an extent similar to Sch9Δ (Figure S3). Interestingly, none of these features were altered in Sch9ΔC2 cells compared to the wild-type (Figures 3(b), (c) and S3 and Table 1).

Deletion of Sch9 is also known to cause a growth defect on galactose, where yeast undergoes intermediate levels of respiration,[1,22] and on non-fermentable carbon sources, such as lactate and ethanol/glycerol.[11] We therefore tested the ability of our Sch9 truncation mutants to grow on poorly- or non-fermentable carbon sources by spotting serial dilutions of liquid cultures on galactose or ethanol/glycerol plates. We observed that the growth defect of Sch9ΔNT on glucose was further exacerbated on galactose media, even though cells grew slightly better than the Sch9Δ control. Moreover, Sch9ΔNT cells were completely unable to grow on ethanol/glycerol plates (Figure 3(d)). Conversely, and in agreement with the phosphorylation and cell cycle duration data, Sch9ΔC2 cells did not present any growth defect on galactose and ethanol/glycerol medium (Figure 3(d)).

In our final test, we explored the capability of our mutant strains to recover after treatment with rapamycin, a potent inhibitor of TORC1.[23] In line with our previous observations, Sch9Δ and Sch9ΔNT cells displayed a similarly strong rapamycin recovery defect, in stark contrast to Sch9ΔC2 cells, whose recovery was indistinguishable from the wild-type (Figure 3(e)).

Based on the evidence presented above, we can therefore conclude that abrogation of Sch9 vacuolar localization via deletion of its N-terminal domain causes severe defects in the downstream stimulation of cell growth, while deletion of the C2 domain has no apparent effect on signaling downstream of Sch9 under the tested growth conditions.

Artificial tethering of Sch9ΔNT at the vacuole restores TORC1-dependent phosphorylation and cell division rate

Given that delocalization of Sch9 from vacuoles appeared to have a detrimental effect on Sch9 activity and cell growth, we asked whether artificial tethering of the Sch9ΔNT mutant at the vacuolar membrane could rescue any of the observed phosphorylation and growth defects caused by the truncation. To do this, we replaced the N-terminal

domain of Sch9 with the vacuolar membrane protein Vac8[24] to create *VAC8*-Sch9ΔNT. Vac8 targeting to the vacuole is TORC1-independent, since Vac8 localization is unaltered after rapamycin treatment, as reported in the CYCLoPs database (https://thecellvision.org/gene/5076/).[25] As expected, Vac8-Sch9ΔNT was fully localized on the vacuolar membrane (Figure S4). We then examined TORC1-dependent phosphorylation, cell cycle duration and growth on galactose and ethanol/glycerol, as well as rapamycin recovery capacity. We found that Vac8-mediated vacuolar tethering restored TORC1-dependent Sch9 phosphorylation (Figure 4(a)) to wild-type levels, enabled cells to grow on galactose and ethanol/glycerol as efficiently as the wild-type (Figure 4(d)), and led to an improved rapamycin recovery compared to Sch9ΔNT (Figure 4(e)). Microscopic observation of *VAC8*-Sch9ΔNT cells further showed that the tethering restored the inter-division time of mothers and the G1 duration of daughters close to wild-type levels (Figure 4(b), (c) and Table1). On the other hand, the volume of daughter cells at birth and budding remained close to the Sch9Δ levels (Figure S3), which suggests that not all Sch9 functions could be restored in this strain. This finding is not surprising, given that Vac8 is a protein that is stably anchored to the vacuole,[24] and prevents Sch9 from moving to the cytoplasm (or the nucleus), where it may have additional functions.

Phosphomimetic mutations at the TORC1 phosphorylation sites of Sch9ΔNT rescue growth defects caused by the N-terminal truncation

Our finding that *VAC8*-Sch9ΔNT can reverse the growth defects of Sch9ΔNT supports the notion that Sch9 needs to localize on the vacuole in order to be activated via phosphorylation by TORC1. If this hypothesis were true, generating a constitutively active (TORC1-independent) form of Sch9ΔNT, should rescue the growth defects caused by N-terminal truncation, and result in a growth phenotype that resembles the wild-type. To generate such a mutant, we introduced phosphomimetic mutations at five TORC1 sites at the C-terminus of Sch9ΔNT. These mutations have been shown to produce a full-length Sch9 mutant (Sch9^{2D3E}) whose activity is independent of TORC1.[1]

Microscopic observation of cells carrying the constitutively active truncated mutant (Sch9ΔNT^{2D3E}) showed that the inter-division time of mothers and G1 duration of daughters were indistinguishable from the corresponding parameters of the Sch9^{2D3E} strain and very close to wild-type levels (Figure 5(a), (b)). At the same time, Sch9^{2D3E} cells displayed a small daughter size which was similar to the size of Sch9ΔNT daughters, indicating that this phosphomimetic mutant is not as active as phosphorylated wild-
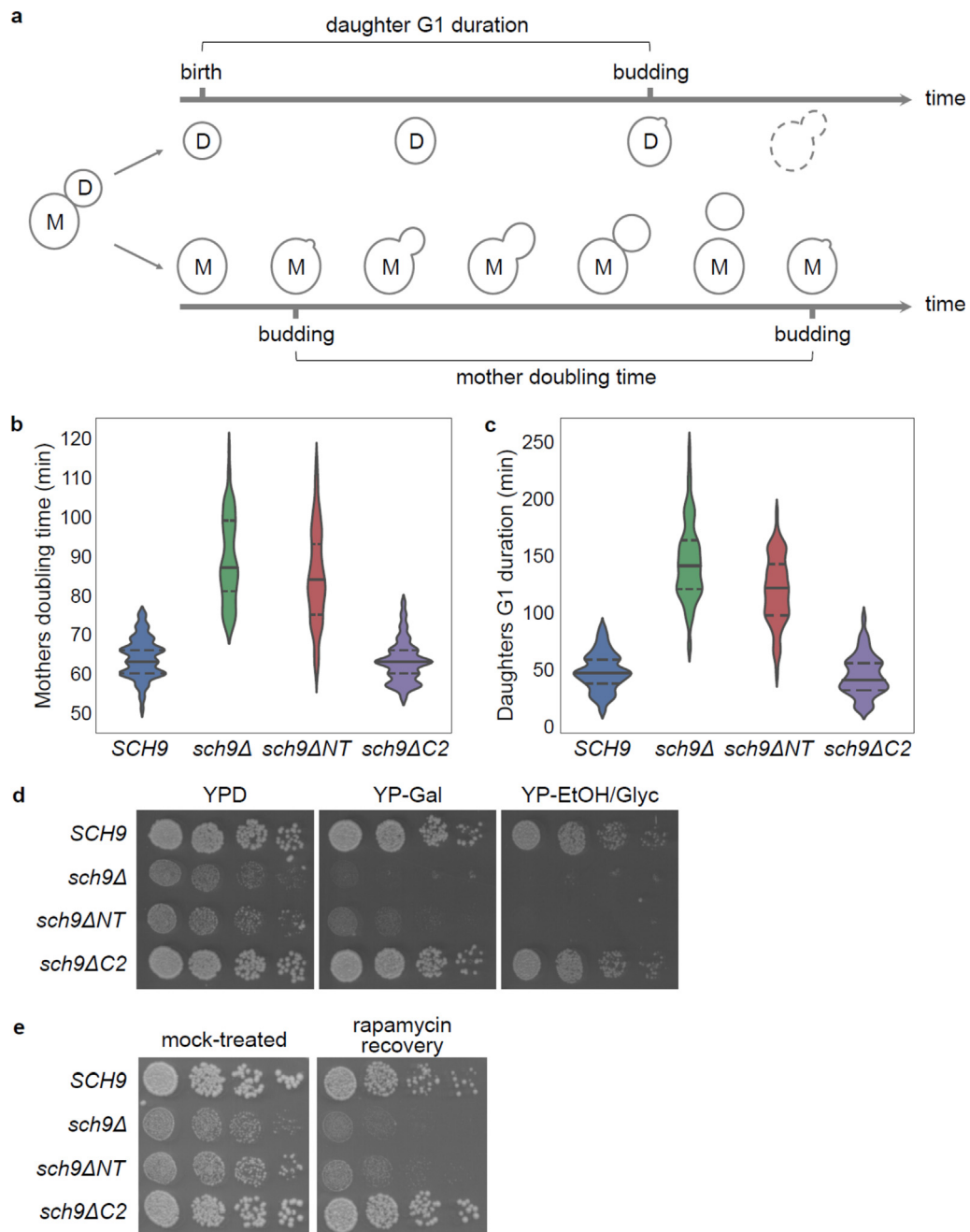
Figure 3. Deletion of the N-terminal domain of Sch9 causes growth defects and impairs recovery from rapamycin treatment. (a) Schematic representation of cell cycle events of mother (M) and daughter (D) cells, highlighting the time intervals analyzed in the single-cell microscopy experiments. The doubling time of mother cells was defined as the interval between two consecutive budding events. The G1 duration of daughters was defined as the time between birth (detachment from the mother cell) and the first budding event. The cell size of daughter cells at birth and at budding for all tested strains is reported in Figure S3. (b), (c) Single cells from the indicated exponentially growing cultures (in YPD medium) were analyzed by time-lapse microscopy. The doubling time of mother cells (b) and the G1 duration of daughter cells (c) is shown. For each strain, at least 85 cell cycles of mother cells and at least 80 cell cycles of daughter cells were analyzed. For each distribution, the median is indicated by a continuous line, and the 25th and 75th percentiles are indicated by dashed lines. Statistical comparisons between strains (p-values and effect sizes) are provided in Supplementary Tables 4 and 5. (d) Serial dilutions of the indicated strains were spotted on YPD, YP-Gal or YP-EtOH/Glyc plates and imaged after 2 (YPD, YP-Gal) or 3 days (YP-EtOH/Glyc) of growth. (e) The indicated strains were mock-treated or treated with rapamycin (200 ng/ml) for 5 h. Serial dilutions were then spotted on (rapamycin-free) YPD plates and imaged after 2 days of growth.
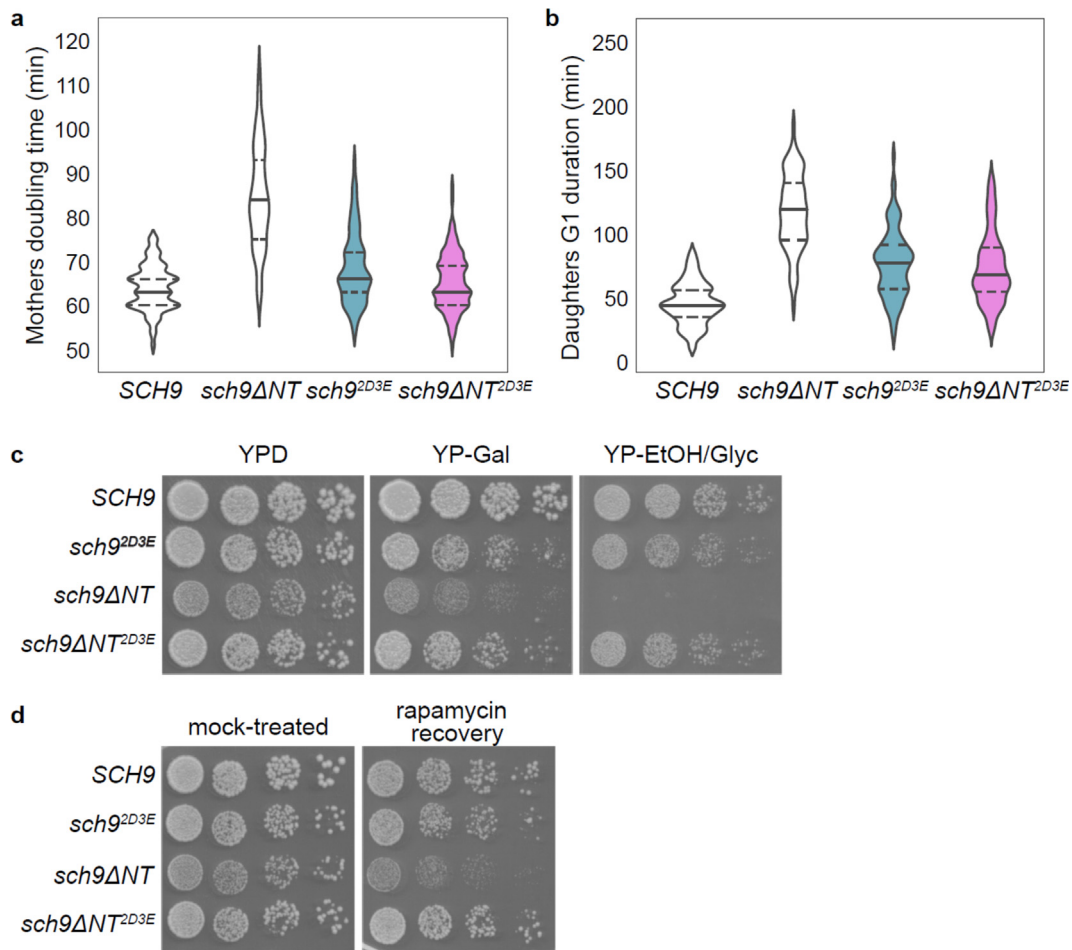
Table 1 Doubling time of mother cells and G1 duration of daughter cells of Sch9 truncation mutants.

genotype	doubling time of mothers [median* (N of cell cycles)]	G1 duration of daughters [median* (N of cell cycles)]
Sch9	63 min (N = 86)	48 min (N = 96)
Sch9Δ	87 min (N = 94)	138 min (N = 85)
Sch9ΔNT	84 min (N = 85)	120 min (N = 80)
Sch9ΔC2	63 min (N = 103)	42 min (N = 91)
VAC8-Sch9ΔNT	66 min (N = 94)	67 min (N = 92)
Sch9^{2D3E}	66 min (N = 115)	78 min (N = 90)
Sch9ΔNT^{2D3E}	63 min (N = 113)	69 min (N = 107)

* Based on a sampling interval of 3 minutes.
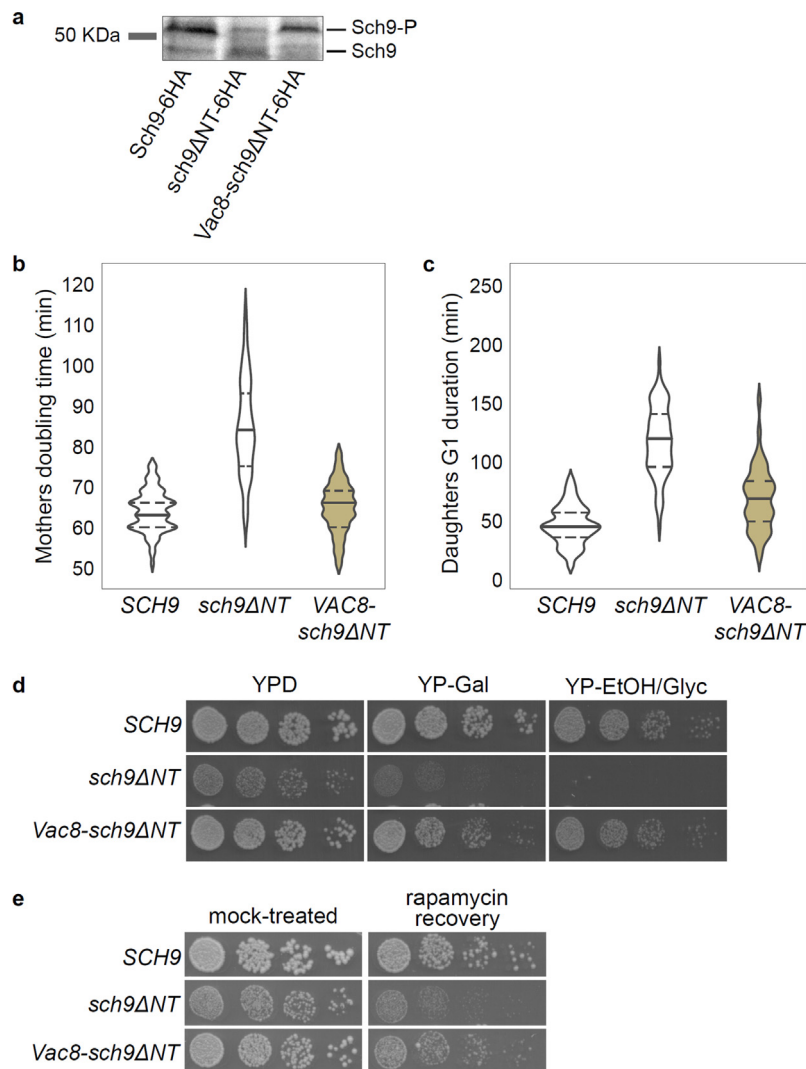
Figure 4. Artificial tethering of Sch9ΔNT at the vacuole rescues TORC1-dependent phosphorylation and cell growth defects and allows partial recovery from rapamycin. (a) The Sch9 phosphorylation status of the indicated strains was analyzed as indicated in Figure 2b. (b), (c) Doubling time of mother cells (b) and G1 duration of daughter cells (c) for the indicated strains, analyzed as indicated in Figure 3(b), (c). Data for strains Sch9 and Sch9ΔNT are the same as plotted in Figure 3(b), (c) and are repeated here to facilitate comparisons. Statistical comparisons between strains (p-values and effect sizes) are provided in Supplementary Tables 4 and 5. d) Growth of the indicated strains on YPD, YP-Gal or YP-EtOH/Glyc plates was analyzed as described in Figure 3(d). (e) The rapamycin recovery capacity of the indicated strains was analyzed as described in Figure 3(e). Images for strains Sch9 and Sch9ΔNT are the same as shown in Figure 3(e), since the *Vac8-*Sch9ΔNT strain was analyzed in the same experiment.

Figure 5. Phosphomimetic mutations on Sch9ΔNT rescue cell growth defects and allow recovery from rapamycin. (a), (b) Doubling time of mother cells (a) and G1 duration of daughter cells (b) for the indicated strains, analyzed as indicated in Figure 3(b), (c). Data for strains Sch9 and Sch9ΔNT are the same as plotted in Figure 3(b), (c) and are repeated here to facilitate comparisons. Statistical comparisons between strains (p-values and effect sizes) are provided in Supplementary Tables 4 and 5. c) Growth of the indicated strains on YPD, YP-Gal or YP-EtOH/Glyc plates was analyzed as described in Figure 3(d). (d) The rapamycin recovery capacity of the indicated strains was analyzed as described in Figure 3(e).

type Sch9. Therefore, although Sch9ΔNT^{2D3E} daughters were indistinguishable from Sch9^{2D3E} daughters in terms of size (Figure S3), we could not assess if the phosphomimetic mutations are able to rescue the cell size defect of daughter cells caused by the N-terminal truncation.

Given the behavior of Sch9ΔNT^{2D3E} cells under the microscope, we proceeded to test their growth on galactose and ethanol/glycerol, as well as their capacity to recover from rapamycin treatment. In these tests, the Sch9ΔNT^{2D3E} mutant grew indistinguishably from the wild-type and Sch9^{2D3E}, indicating that the phosphomimetic mutations of the TORC1 sites bypass the requirement for vacuolar localization of the kinase. In turn, this fact suggests that a major function of Sch9 vacuolar localization is to bring Sch9 in contact with TORC1 in order to be activated by phosphorylation.

Discussion

Given the central role of Sch9 in the regulation of cell growth, understanding the key determinants of Sch9 activity is essential for untangling the complex signaling pathways in which Sch9 is embedded. Although it had been previously shown that the first 390 residues of Sch9 bind to PI(3,5) P2 *in vitro*,[18] it was hypothesized that this interaction was mediated by the C2 domain of Sch9 (residues 183-399). Our results suggest that the N-terminal domain of the protein (residues 1-182) is necessary for binding to the vacuole (although we did not test the direct interaction of this domain with the phospholipids), while the C2 domain is dispensable (Figures 1 and S1). While this manuscript was in preparation, a study was published that confirmed our observations on the *in vivo* localization of Sch9 truncation mutants, and showed that the

N-terminal domain of Sch9 preferentially interacts *in vitro* with PI(3,5)P2 and localizes on the vacuole *in vivo*.[26] It will be interesting to elucidate the mechanism of this interaction, since the N-terminal domain of Sch9 does not seem to correspond to any known lipid-binding domain. Interestingly, the same study observed that an Sch9 fragment consisting of the N-terminal domain alone localizes also to perivacuolar dots, corresponding to signaling endosomes, in a PI(3,5)P2-dependent manner, while full-length Sch9 localizes exclusively at the vacuolar surface and in the cytoplasm. Future studies will be needed to investigate why full-length Sch9 is targeted specifically to the vacuole and not to endosomes.

Recent work had shown that Sch9 has specific functions on the vacuole,[13,14] which suggested that the ability of Sch9 to bind to the vacuolar membrane is necessary for signal transduction downstream of Sch9. However, previous studies had induced delocalization of Sch9 via disruption of intracellular trafficking[20] or phospholipid synthesis,[18] which made it difficult to study the consequences of the delocalization itself, since these genetic perturbations affect many pathways besides Sch9 signaling. By studying the Sch9ΔNT strain which is specifically defective in Sch9 localization, we showed that loss of the vacuolar localization of Sch9 leads to loss of TORC1-dependent phosphorylation and growth defects which resemble the Sch9Δ phenotype. Therefore, our results clearly demonstrate that contact of Sch9 with the vacuole (at least transiently) is necessary for proper activation and function of the kinase, while not excluding that it may have additional functions at other intracellular locations.

While loss of the N-terminal domain of Sch9 has a clear effect on Sch9 localization, phosphorylation and activity, the loss of the C2 domain does not appear to negatively affect Sch9 localization, phosphorylation by TORC1, or any of the growth-related features that we examined via our microscopy and spot assays (Figures 2, 3 and S3 and Table 1). It should be noted that the Sch9 C2 domain appears to have low similarity to typical C2 domain sequences, and lacks the full complement of Ca^{2+}-coordinating residues found in many phospholipid-binding C2 domains.[27] It will be interesting to uncover what is the function of this C2 domain, and under which conditions it becomes important. One possibility is that the C2 domain of Sch9 mediates interaction with a protein partner instead of phospholipid binding, as has been observed for other C2 domains.[28–31] Intriguingly, the Sch9ΔC2 strain appears more resistant to rapamycin compared to wild-type (Figure S2), suggesting that Sch9ΔC2 may even be more active than the wild-type protein, for example due to impaired dephosphorylation, or relief of autoinhibition, as in the case of PKC.[31]

Our findings suggest that Sch9 is still able to encounter many of its substrates while localized on the vacuole, as *VAC8*-Sch9ΔNT was able to restore most of the wild-type growth features that were altered in the Sch9ΔNT mutant (Figure 4). According to the same evidence, the N-terminal domain of Sch9 appears to only be necessary for the proper localization of the protein. The recent demonstration that this domain can bind the signaling lipid PI(3,5)P2[26] lends further support to this notion. On the other hand, the surprising rescue of growth defects of Sch9ΔNT by the constitutively active truncated mutant (Sch9ΔNT^{2D3E}) provides a strong indication that the key function of the Sch9 vacuolar localization is to facilitate the Sch9-TORC1 contact, which results in the activation of the former via phosphorylation by the latter under favorable growth conditions. At the same time, the fact that fully vacuolar Sch9 (*VAC8*-Sch9ΔNT) cannot restore all Sch9 functions, suggests that Sch9 cycles between vacuole and cytoplasm. This localization-dependent activation mode of Sch9 provides a mechanistic basis for the specific modulation of the Sch9 branch of TORC1 signaling, since it is known that yeast cells can modify the abundance of PI(3,5)P2 on the vacuole in response to stress,[20] and thus regulate the subcellular distribution of Sch9. Our findings therefore provide new mechanistic insights into the spatial regulation of a major TORC1 signaling branch, by elucidating the connections between localization, phosphorylation and downstream activity of Sch9.

Materials and Methods

Yeast strains and growth conditions

Standard yeast media and growth conditions were used.[32] All yeast strains used in this study were constructed in the S288C-derived prototrophic genetic background YSBN6[33] and are listed in Supplementary Table 1. Strains yDN68.1, yDN69.1, yDN70.1, yDN16.1, yDN17.1, yDN52.2, yDN97.2 and yDN105.1 were obtained by integrating the NotI-digested plasmids pYTK211, pYTK212, pYTK213, pYTK128, pYTK145, pYTK191, pYTK230 and pYTK232, respectively, at the HO locus in YSBN6. The integration was verified by sequencing. To construct strain YSBN6 Sch9^{2D3E}, the sequence of Sch9^{2D3E} (T723D, S726D, T737E, S758E, S765E) was PCR-amplified from plasmid pJU841[1] with primers Sch9_2D3E_cds_fwd and Sch9_2D3E_cds_rev and transformed in strain YSBN6 Hta2-mRFP.[34] Strains yDN85.3, yDN86.1, yDN87.1, yDN94.3 and yDN104.1 were constructed using CRISPR/Cas9 technology[35,36] by co-transforming YSBN6 (or YSBN6 Sch9^{2D3E} for yDN104.1) with the sgRNA- and Cas9-containing plasmids pYTK106 (for yDN86.1, yDN94.3 and yDN104.1) or pYTK107 (for yDN85.3 and yDN87.1) and the proper repair fragment. The repair fragment for yDN85.3 was obtained by PCR-amplification of partially overlapping oligonucleotides Sch9del_rep-for / Sch9del_rep-rev. The repair fragment for yDN86.1 and yDN104.1 was obtained by PCR-amplification of partially overlapping oligonucleotides Sch9_NTdel_rep-for / Sch9_NTdel_rep-rev. The repair fragment for yDN87.1 was obtained by PCR amplification from plasmid pYTK145 with primers Sch9-NT-for and Sch9-int-rev. The repair fragment for yDN94.3 was obtained by amplification of *VAC8* from pRH2776[37] with primers VAC8-rep-for and VAC8-rep-rev. Plasmids pYTK106 and pYTK107 were subsequently eliminated by growing overnight cultures in non-selective medium and plat-

ing for single colonies on non-selective plates. Plasmid loss was verified by inability to grow on YPD + NAT plates. The desired genome editing event was verified by sequencing.

For strains yDN94.3 and yDN104.1, the *IRA1* and *IRA2* genes were fully sequenced to exclude that the observed phenotypic rescue is due to the accumulation of suppressor mutations.[11]

Plasmid construction

All plasmids were constructed with the MoClo-YTK[35] and are listed in Supplementary Table 2.

New part plasmids. New parts were PCR-amplified and cloned in entry vector pYK001 via BsmBI Golden Gate assembly. To generate pYTK111 (Sch9-part-4a), the Sch9 sequence was amplified from the yeast genome in 4 fragments to remove BsaI and BsmBI restriction sites via introduction of synonymous mutations ("domestication"), using the following primers: Sch9-YTK-4a-for and Sch9-A-rev, Sch9-B-for and Sch9-B-rev, Sch9-C-for and Sch9-C-rev, Sch9-D-for and Sch9-YTK-4a-rev. pYTK123 (Sch9-part-3) was generated by amplification of Sch9 from pYTK111 using primers Sch9-YTK-3-for and Sch9-YTK-3-rev. pYTK136 (Sch9*NT*-part-3a) was generated by amplification of Sch9$^{aa1\text{-}182}$ from pYTK111 using primers Sch9-YTK-3-for and Sch9-NT-3a-rev. pYTK137 (Sch9*NT*-part-3b) was generated by amplification of Sch9$^{aa1\text{-}182}$ from pYTK111 using primers Sch9-NT-3b-for and Sch9-NT-3b-rev. pYTK138 (Sch9*CT*-part-3b) was generated by amplification of Sch9$^{aa400\text{-}824}$ from pYTK111 using primers Sch9-CT-3b-for and Sch9-YTK-3-rev. pYTK139 (Sch9*CT*-part-4a) was generated by amplification of Sch9$^{aa400\text{-}824}$ from pYTK111 using primers Sch9-CT-4a-for and Sch9-CT-4a-rev. pYTK189 (Sch9*ΔNT*-part-3) was generated by amplification of Sch9$^{aa183\text{-}824}$ from pYTK111 using primers Sch9-C2-3-for and Sch9-YTK-3-rev. pYTK205 (Sch9*ΔNT*-part-3b) was generated by amplification of Sch9$^{aa183\text{-}824}$ from pYTK111 using primers Sch9-C2-3b-for and Sch9-YTK-3-rev. pYTK215 (Sch9*ΔNT*-part-4a) was generated by amplification of Sch9$^{aa183\text{-}824}$ from pYTK111 using primers Sch9-C2-4-for and Sch9-CT-4a-rev. pYTK109 (pSch9-part-2) was generated by amplification of 535 bps upstream of the Sch9 ORF from the yeast genome using primers Sch9p-YTK-2-for and Sch9p-YTK-2-rev. pYTK126 (*6HA*-part-4a) was generated by amplification of the *6HA* sequence from pHyg-AID*-6HA (Addgene #99520) using primers HA-YTK-4a-for and HA-YTK-4a-rev. To generate pYTK227 (*VAC8*-part-3), the *VAC8* sequence was amplified from pRH2776[37] in 2 fragments to remove a BsaI restriction site via introduction of a synonymous mutation ("domestication"), using the following primers: VAC8-YTK-3-for and VAC8-A-rev, VAC8-B-for and VAC8-linker-YTK-3a-rev. All new cloned parts were verified by sequencing.

Integration vector. GFP-dropout HO-locus integration vector pYTK163 was generated by BsaI Golden Gate assembly of parts pYTK002 + pYTK047 + pYTK067 + pYTK077 + pYTK088 + pYTK089 + pYTK094.

Cassette plasmids. pYTK211 was generated by BsaI Golden Gate assembly of parts pYTK021 + pYTK033 + pYTK111 + pYTK064 + pYTK163. pYTK212 was generated by BsaI Golden Gate assembly of parts pYTK021 + pYTK038 + pYTK137 + pYTK139 + pYTK064 + pYTK163. pYTK213 was generated by BsaI Golden Gate assembly of parts pYTK021 + pYTK038 + pYTK205 + pYTK054 + pYTK163. pYTK128 was generated by BsaI Golden Gate assembly of parts pYTK109 + pYTK123 + pYTK126 + pYTK061 + pYTK163. pYTK145 was generated by BsaI Golden Gate assembly of parts pYTK109 + pYTK136 + pYTK138 + pYTK126 + pYTK061 + pYTK163. pYTK191 was generated by BsaI Golden Gate assembly of parts pYTK109 + pYTK189 + pYTK126 + pYTK061 + pYTK163. pYTK230 was generated by BsaI Golden Gate assembly of parts pYTK109 + pYTK227 + pYTK205 + pYTK126 + pYTK061 + pYTK163.

pYTK232 was generated by BsaI Golden Gate assembly of parts pYTK021 + pYTK227 + pYTK045 + pYTK215 + pYTK064 + pYTK163.

CRISPR/Cas9 plasmids. Plasmids expressing a single guide RNA (sgRNA) and Cas9 were constructed as indicated in refs 35 and 36.[35,36] Sch9-sgRNA1 (GTATCCGTTGTCGTTGC-CAGCGG) and Sch9-sgRNA2 (GGCCTAAGAACA-TATGGTCGTGG) were cloned in pYTK050 via BsmBI Golden Gate assembly of partially overlapping oligonucleotides Sch9-sgRNA1-for and Sch9-sgRNA1-rev, and Sch9-sgRNA2-for and Sch9-sgRNA2-rev, respectively. The resulting "sgRNA part plasmids" were then assembled to obtain two "sgRNA cassette plasmids" via BsaI Golden Gate assembly of plasmids pYTK003 + sgRNA part plasmid + pYTK068 + pYTK095. To generate plasmids pYTK106 (Sch9-sgRNA1 + Cas9) and pYTK107 (Sch9-sgRNA2 + Cas9), the sgRNA parts were then combined with Cas9 in a multigene vector via BsmBI Golden Gate assembly of the following plasmids: pYTK104 + sgRNA cassette plasmid + pYTK105 + pYTK102. pYTK104 was obtained by BsaI Golden Gate assembly of parts pYTK002 + pYTK011 + pYTK036 + pYTK054 + pYTK067 + pYTK095. pYTK105 was obtained by BsaI Golden Gate assembly of parts pYTK004 + pYTK048 + pYTK072 + pYTK095. pYTK102 was obtained by BsaI Golden Gate assembly of parts pYTK008 + pYTK047 + pYTK073 + pYTK078 + pYTK081 + pYTK084.

Primers

All primers are listed in Supplementary Table 3.

Microscopy

Fluorescent microscopy was performed with a Zeiss LSM800 confocal microscope and photomultiplier tubes by Hamamatsu Photonics, using YNB agarose slabs perfused in 2% glucose. A 63x Zeiss Plan Apochromat (N.A. = 1.4) oil immersion objective was used. The temperature was kept at 30 °C throughout the experiments using an incubator chamber and a controlled heated objective ring. For Venus and FM4-64 fluorescence detection cells were excited with a 488-nm laser (0.56 µs dwell-time exposure) and emission was detected using a 410 to 585 nm band-pass filter for Venus and a 645 to 700 nm band pass filter for FM4-64. For every imaging position, five z axis planes with a 0.8-µm step were acquired.

Widefield microscopy was performed using an inverted fluorescence microscope (Eclipse Ti-E, Nikon Instruments). Temperature was kept constant at 30 °C using a microscope incubator (Life Imaging Services). For all the experiments a 100x Nikon S Fluor (N.A. = 1.30) objective was used. Images were recorded using iXon Ultra 897 DU-897-U-CD0-#EX cameras (Andor Technology). For the measurement of mother cells doubling time and daughter cells G1 duration and volumes distributions, exponentially growing cells were placed under a pre-warmed agarose pad (YPD + 1% agarose) and loaded under the microscope. For each experiment multiple non-overlapping XY positions were recorded and for each position bright field imaging was performed every 3 minutes. Mother cells doubling time was defined as the time in between two budding events, identified by the appearance of a dark spot on the cell membrane. Daughter cells G1 duration was defined as the time from the detachment of the bud from the mother cell, identified by the darkening of the bud neck, to the first budding event. To measure cell volume distributions, cells were segmented using the semi-automated ImageJ plug-in BudJ.[38] The volume output from BudJ was then used for further analysis.

Protein extraction and Western Blot

Protein extracts were prepared and visualized essentially as described in ref. 1[1] with slight modifications. 10 ml of cell culture

at OD = 0.8 were fixed with TCA (final concentration 6%), kept in ice for at least 10 min, pelleted, washed twice with cold acetone and air dried. Pellets were resuspended in urea buffer (50 mM Tris HCl pH 7.5, 5 mM EDTA, 6 M Urea, 1% SDS, 1 mM PMSF, 1:100 Phosphatase Inhibitor Cocktail 3 [Sigma-Aldrich P0044]) and cells were lysed by bead beating. Samples were incubated for 10 min at 65 °C (shaking at 800 rpm) and centrifuged for 5 min at 15000 rpm at 4 °C (for precipitation of insoluble proteins). For NTCB cleavage, 80 μl of protein extracts were mixed with 24 μl 0.5 M CHES (pH 10.5) and 16 μl 75 mM NTCB and incubated overnight at room temperature. Samples were then mixed with an equal volume of 2X sample buffer (+20 mM TCEP and 1:100 Phosphatase Inhibitor Cocktail 3), boiled 5 minutes at 95 °C, centrifuged for 1 min at 4 °C and run on 12% SDS PAGE gel. Sch9-6HA was visualized via immunoblotting with 12CA5 anti-HA (Santa Cruz Biotechnology, sc-57592) as primary antibody and Goat anti-Mouse HRP (Jackson ImmunoResearch, 115-035-003) as secondary antibody.

Spot assay

Overnight yeast cultures were normalized at OD = 0.2 and 5-fold serial dilutions were spotted on YPD (2% glucose), YP-Gal (2% galactose) or YP-EtOH/Glyc (3% glycerol, 2% ethanol). Images were taken after 2 or 3 days of incubation at 30 °C.

Rapamycin recovery assay

Exponentially growing yeast cultures were normalized to OD = 0.4 and mock- (1% DMSO) or rapamycin-treated (200 ng/ml) for 5 hours. Cells were collected by centrifugation, washed with sterile water and resuspended in sterile water. Cultures were then normalized at OD = 0.2 and 5-fold serial dilutions were spotted on YPD plates and incubated at 30 °C for 2 days.

CRediT authorship contribution statement

Daniele Novarina: Conceptualization, Investigation, Methodology, Resources, Visualization, Writing - original draft, Writing - review & editing. **Paolo Guerra:** Formal analysis, Investigation, Data curation, Visualization. **Andreas Milias-Argeitis:** Conceptualization, Methodology, Supervision, Project administration, Funding acquisition, Writing - original draft, Writing - review & editing.

DECLARATION OF COMPETING INTEREST

The authors declare that they have no known competing financial interests or personal relationships that could have appeared to influence the work reported in this paper.

Acknowledgements

Appendix A. Supplementary Data

References

1. Urban, J., Soulard, A., Huber, A., Lippman, S., Mukhopadhyay, D., Deloche, O., Wanke, V., Anrather, D., et al., (2007). Sch9 is a major target of TORC1 in *Saccharomyces cerevisiae*. *Mol. Cell* **26**, 663–674. https://doi.org/10.1016/j.molcel.2007.04.020.
2. Huber, A., Bodenmiller, B., Uotila, A., Stahl, M., Wanka, S., Gerrits, B., Aebersold, R., Loewith, R., (2009). Characterization of the rapamycin-sensitive phosphoproteome reveals that Sch9 is a central coordinator of protein synthesis. *Genes Dev.* **23**, 1929–1943. https://doi.org/10.1101/gad.532109.
3. Roosen, J., Engelen, K., Marchal, K., Mathys, J., Griffioen, G., Cameroni, E., Thevelein, J.M., De Virgilio, C., et al., (2005). PKA and Sch9 control a molecular switch important for the proper adaptation to nutrient availability. *Mol. Microbiol.* **55**, 862–880. https://doi.org/10.1111/j.1365-2958.2004.04429.x.
4. Pedruzzi, I., Dubouloz, F., Cameroni, E., Wanke, V., Roosen, J., Winderickx, J., De Virgilio, C., (2003). TOR and PKA signaling pathways converge on the protein kinase Rim15 to control entry into G0. *Mol. Cell* **12**, 1607–1613. https://doi.org/10.1016/S1097-2765(03)00485-4.
5. Swinnen, E., Wilms, T., Idkowiak-Baldys, J., Smets, B., De Snijder, P., Accardo, S., Ghillebert, R., Thevissen, K., et al., (2014). The protein kinase Sch9 is a key regulator of sphingolipid metabolism in *Saccharomyces cerevisiae*. *Mol. Biol. Cell* **25**, 196–211. https://doi.org/10.1091/mbc.E13-06-0340.
6. Deprez, M.A., Eskes, E., Winderickx, J., Wilms, T., (2018). The TORC1-Sch9 pathway as a crucial mediator of chronological lifespan in the yeast *Saccharomyces cerevisiae*. *FEMS Yeast Res.* **18**, foy048. https://doi.org/10.1093/femsyr/foy048.
7. Kaeberlein, M., Westman, E., Dang, N., Kerr, E., Powers III, R., Steffen, K., Hu, D., Kennedy, B., et al., (2005). Regulation of yeast replicative life span by TOR and Sch9 in response to nutrients. *Science (80-.)* **310**, 1193–1196. https://doi.org/10.1126/science.1115535.

8. Loewith, R., Hall, M.N., (2011). Target of rapamycin (TOR) in nutrient signaling and growth control. *Genetics* **189**, 1177–1201. https://doi.org/10.1534/GENETICS.111.133363.

9. Jorgensen, P., Tyers, M., (2004). How cells coordinate growth and division. *Curr. Biol.* **14**, R1014–R1027. https://doi.org/10.1016/j.cub.2004.11.027.

10. Jorgensen, P., Nishikawa, J.L., Breitkreutz, B.J., Tyers, M., (2002). Systematic identification of pathways that couple cell growth and division in yeast. *Science (80-.)* **297**, 395–400. https://doi.org/10.1126/science.1070850.

11. Peterson, P.P., Liu, Z., (2021). Identification and characterization of rapidly accumulating Sch9Δ suppressor mutations in *Saccharomyces cerevisiae. G3 Genes|Genomes|Genet.* **11**, jkab134. https://doi.org/10.1093/g3journal/jkab134.

12. Jorgensen, P., Rupeš, I., Sharom, J.R., Schneper, L., Broach, J.R., Tyers, M., (2004). A dynamic transcriptional network communicates growth potential to ribosome synthesis and critical cell size. *Genes Dev.* **18**, 2491–2505. https://doi.org/10.1101/gad.1228804.

13. Jin, Y., Weisman, L.S., (2015). The vacuole/lysosome is required for cell-cycle progression. *Elife* **4**, e08160. https://doi.org/10.7554/eLife.08160.

14. Wilms, T., Swinnen, E., Eskes, E., Dolz-Edo, L., Uwineza, A., Van Essche, R., Rosseels, J., Zabrocki, P., et al., (2017). The yeast protein kinase Sch9 adjusts V-ATPase assembly/disassembly to control pH homeostasis and longevity in response to glucose availability. *PLoS Genet.* **13**, e1006835. https://doi.org/10.1371/journal.pgen.1006835.

15. Prouteau, M., Desfosses, A., Sieben, C., Bourgoint, C., Mozaffari, N.L., Demurtas, D., Mitra, A.K., Guichard, P., et al., (2017). TORC1 organized in inhibited domains (TOROIDs) regulate TORC1 activity. *Nature* **550**, 265–269. https://doi.org/10.1038/nature24021.

16. Hughes Hallett, J.E., Luo, X., Capaldi, A.P., (2015). Snf1/AMPK promotes the formation of Kog1/raptor-bodies to increase the activation threshold of TORC1 in budding yeast. *Elife* **4**, e09181. https://doi.org/10.7554/eLife.09181.

17. Kira, S., Kumano, Y., Ukai, H., Takeda, E., Matsuura, A., Noda, T., (2016). Dynamic relocation of the TORC1-Gtr1/2-Ego1/2/3 complex is regulated by Gtr1 and Gtr2. *Mol. Biol. Cell* **27**, 382–396. https://doi.org/10.1091/mbc.E15-07-0470.

18. Jin, N., Mao, K., Jin, Y., Tevzadze, G., Kauffman, E.J., Park, S., Bridges, D., Loewith, R., et al., (2014). Roles for PI(3,5)P2 in nutrient sensing through TORC1. *Mol. Biol. Cell* **25**, 1171–1185. https://doi.org/10.1091/mbc.E14-01-0021.

19. Lemmon, M.A., (2008). Membrane recognition by phospholipid-binding domains. *Nature Rev. Mol. Cell Biol.* **9**, 99–111. https://doi.org/10.1038/nrm2328.

20. Takeda, E., Jin, N., Itakura, E., Kira, S., Kamada, Y., Weisman, L.S., Noda, T., Matsuura, A., (2018). Vacuole-mediated selective regulation of TORC1-Sch9 signaling following oxidative stress. *Mol. Biol. Cell* **29**, 510–522. https://doi.org/10.1091/mbc.E17-09-0553.

21. Vida, T.A., Emr, S.D., (1995). A new vital stain for visualizing vacuolar membrane dynamics and endocytosis in yeast. *J. Cell Biol.* **128**, 779–792. https://doi.org/10.1083/jcb.128.5.779.

22. Fendt, S.M., Sauer, U., (2010). Transcriptional regulation of respiration in yeast metabolizing differently repressive carbon substrates. *BMC Syst. Biol.* **4**, 12. https://doi.org/10.1186/1752-0509-4-12.

23. Evans, S.K., Burgess, K.E.V., Gray, J.V., (2014). Recovery from rapamycin: Drug-insensitive activity of yeast Target of Rapamycin Complex 1 (TORC1) supports residual proliferation that dilutes rapamycin among progeny cells. *J. Biol. Chem.* **289**, 26554–26565. https://doi.org/10.1074/JBC.M114.589754.

24. Wang, Y.X., Catlett, N.L., Weisman, L.S., (1998). Vac8p, a vacuolar protein with armadillo repeats, functions in both vacuole inheritance and protein targeting from the cytoplasm to vacuole. *J. Cell Biol.* **140**, 1063–1074. https://doi.org/10.1083/jcb.140.5.1063.

25. Koh, J.L.Y., Chong, Y.T., Friesen, H., Moses, A., Boone, C., Andrews, B.J., Moffat, J., (2015). CYCLoPs: A comprehensive database constructed from automated analysis of protein abundance and subcellular localization patterns in *Saccharomyces cerevisiae. G3/Genes/Genomes/Genet.* **5**, 1223–1232. https://doi.org/10.1534/g3.115.017830.

26. Chen, Z., Malia, P.C., Hatakeyama, R., Nicastro, R., Hu, Z., Péli-Gulli, M.P., Gao, J., Nishimura, T., et al., (2021). TORC1 determines Fab1 lipid kinase function at signaling endosomes and vacuoles. *Curr. Biol.* **31**, 297–309.e8. https://doi.org/10.1016/j.cub.2020.10.026.

27. Nalefski, E.A., Falke, J.J., (1996). The C2 domain calcium-binding motif: Structural and functional diversity. *Protein Sci.* **5**, 2375–2390. https://doi.org/10.1002/pro.5560051201.

28. Benes, C.H., Wu, N., Elia, A.E.H., Dharia, T., Cantley, L.C., Soltoff, S.P., (2005). The C2 domain of PKCδ is a phosphotyrosine binding domain. *Cell* **121**, 271–280. https://doi.org/10.1016/j.cell.2005.02.019.

29. Chen, S., Jiao, L., Shubbar, M., Yang, X., Liu, X., (2018). Unique structural platforms of Suz12 dictate distinct classes of PRC2 for chromatin binding. *Mol. Cell* **69**, 840–852.e5. https://doi.org/10.1016/j.molcel.2018.01.039.

30. Wang, T., Pentyala, S., Elliott, J.T., Dowal, L., Gupta, E., Rebecchi, M.J., Scarlata, S., (1999). Selective interaction of the C2 domains of phospholipase C-β1 and -β2 with activated Gαq subunits: An alternative function for C2-signaling modules. *Proc. Natl. Acad. Sci. USA* **96**, 7843–7846. https://doi.org/10.1073/pnas.96.14.7843.

31. Antal, C.E., Callender, J.A., Kornev, A.P., Taylor, S.S., Newton, A.C., (2015). Intramolecular C2 domain-mediated autoinhibition of Protein Kinase C βII. *Cell Rep.* **12**, 1252–1260. https://doi.org/10.1016/j.celrep.2015.07.039.

32. Sherman, F., (2002). Getting started with yeast. *Methods Enzymol.* **350**, 3–41. https://doi.org/10.1016/S0076-6879(02)50954-X.

33. Canelas, A.B., Harrison, N., Fazio, A., Zhang, J., Pitkänen, J.P., Van Den Brink, J., Bakker, B.M., Bogner, L., et al., (2010). Integrated multilaboratory systems biology reveals differences in protein metabolism between two reference yeast strains. *Nature Commun.* **1**, 145. https://doi.org/10.1038/ncomms1150.

34. Guerra, P., Vuillemenot, L.-A.P.E., Been, M., Milias-Argeitis, A., (2021). TORC1 and PKA activity towards ribosome biogenesis oscillates in synchrony with the budding yeast cell cycle. *BioRxiv*. https://doi.org/10.1101/2021.05.31.446450.

35. Lee, M.E., DeLoache, W.C., Cervantes, B., Dueber, J.E., (2015). A highly characterized yeast toolkit for modular,

multipart assembly. *ACS Synth. Biol.* **4**, 975–986. https://doi.org/10.1021/sb500366v.

36. Akhmetov, A., Laurent, J., Gollihar, J., Gardner, E., Garge, R., Ellington, A., Kachroo, A., Marcotte, E., (2018). Single-step precision genome editing in yeast using CRISPR-Cas9. *BIO-PROTOCOL.* **8**, e2765. https://doi.org/10.21769/bioprotoc.2765.

37. Powis, K., Zhang, T., Panchaud, N., Wang, R., De Virgilio, C., Ding, J., (2015). Crystal structure of the Ego1-Ego2-Ego3 complex and its role in promoting Rag GTPase-dependent TORC1 signaling. *Cell Res.* **25**, 1043–1059. https://doi.org/10.1038/cr.2015.86.

38. Ferrezuelo, F., Colomina, N., Palmisano, A., Garí, E., Gallego, C., Csikász-Nagy, A., Aldea, M., (2012). The critical size is set at a single-cell level by growth rate to attain homeostasis and adaptation. *Nature Commun.* **3**, 1012. https://doi.org/10.1038/ncomms2015.